

# Characterization of Materials for Advanced techniques required for Optical Communication Systems Engineering

CHRIS MAY<sup>1</sup>

<sup>1</sup>Master's Internship Program, 1252 University of Oregon, Eugene, OR 97403

\*Corresponding author: cmay7@uoregon.edu

Compiled August 7, 2018

Advanced topics in optics are explored to better understand the requirements for high efficiency optical communications. The Laguerre-Gaussian modes of an open cavity Helium Neon laser are documented and explored. The beam waist and divergence for light propagating through an optical fiber are measured to be around  $160\mu\text{m}$  with a Rayleigh range of  $1.306\text{mm}$  and a coupling efficiency near 27% is achieved. Also two acousto-optic modulators are characterized to solve for the speed of sound in their respective crystals as  $v_s \approx 3500[\text{m/s}]$  and  $v_s \approx 8000[\text{m/s}]$ .

<http://dx.doi.org/10.1364/ao.XX.XXXXXX>

## 1. INTRODUCTION

One of the most interesting solutions to the Helmholtz equations involves solving this very versatile equation in cylindrical coordinates. A generic approach leads to Bessel function solutions with the assistance of Frobenius' method, but the use of a Gaussian "ansatz" leads to Laguerre-Gaussian solutions which have very interesting properties. These beams lead to lasing within cavities, and in these cavities many different Laguerre-Gauss modes can exist. These modes can also be propagated into optical fibers to send signals across long distances at the speed of light with much less power than conventional radio. The ability to send these signals leads to a desire to modulate signals to avoid data loss while propagating on the fiber.

In this document is a discussion on some of the properties which govern the creation of laser light which can be used for optical communication. This will be followed by the characterization of an optical fiber and the challenges involved with propagating high efficiency signals for a single mode fiber. To finish up a method for encoding messages into optical fibers will be explored with an acousto-optic modulator.

## 2. OPEN CAVITY HE-NE LASER

### A. Obtaining Lasing

#### A.1. Theory

One of the simplest diagrammatic methods to view a laser is to consider it as a Fabry-Perot interferometer. The general idea is that energy is pumped into a steady state system which causes electrons to be bumped up into higher orbitals which are unstable, whereupon they drop into lower energy states and emit

photons which cause a chain reaction where further coherent photons will be produced through a similar process [1].

If the light which is constantly being emitted from the material is prepared within a Fabry-Perot interferometer then it will continuously reflect off the surfaces which results in a high energy beam which continues to stimulate the material and lasing begins. The beam which is emitted has a Gaussian shape, and to prevent beam walk-off and get the highest efficiency possible from the laser spherical mirrors which match the Gaussian modes can be used to form the Fabry-Perot cavity [2].

The open cavity He-Ne laser is a plastic box which contains a tube full of Helium and Neon gas. A power source can be used to excite electrons in the gas and cause fluorescence which propagates along an optical axis in Gaussian modes.

#### A.2. Methods

The plastic box containing the laser was placed on an optical rail. The total length of the box is about  $30\text{cm}$  and from the rear of the box to the front of the HeNe tube was about  $27\text{cm}$ . The optical coupler was placed on the rail and moved from the far right end toward the box. Lasing was initially observed at about  $47.1\text{cm}$  from the box, and the beam remained lasing under the condition of proper alignment of the coupler with the fluorescent beam.

The cavity is filled with HeNe gas particles that are very close, so the mean free path in the cavity is probably significantly shorter than for particles which are located outside of the cavity. The shorter mean free path would correspond to a higher amount of scattering, and thus more light emanating from the cavity in comparison to the air outside.

## B. Mirror Curvatures

### B.1. Theory

The spherical mirrors have a limited range of angles through which they can reflect light which is related to their radius of curvature. This leads to the beam confinement condition [3].

$$0 \leq \left(1 + \frac{d}{R_1}\right) \left(1 + \frac{d}{R_2}\right) \leq 1 \quad (1)$$

The term  $d$  is the distance between the two mirrors, while the term  $R_1$  is the radius of curvature for one mirror and  $R_2$  is the radius of curvature for the second mirror. Outside of this region of stability lasing cannot occur, because the reflected beams will diverge from the opposite mirror.

### B.2. Methods

The optical coupler was placed as near to the cavity as possible which was based off the dimensions of the plastic container. To determine the range where lasing can occur the coupler was moved down the optical rail until a point was reached where lasing would end. One of the challenging aspects of this approach was that the orientation of the translating spherical mirror would change, and lasing could end due to a misalignment. A method which would be better would be to create a feedback system which measures the output intensity of the beam and rotates the mirror when it starts to become misaligned.

### B.3. Results

When translating the optical coupler along the rail it seemed as if the device was capable of lasing from the location of the box all the way out to a distance about 95cm from the edge of the box. This makes it challenging because there are two unknowns and only a single value to work with. Due to this constraint the assumption (which is incorrect) that the mirrors are identical in curvature can be made, which reduces Eq. 1 to,

$$0 \leq \frac{-d}{R} \leq 2$$

Which means that the radii of curvature of the two mirrors can be solved as,

$$R = -\frac{d}{2} = -42.5 \pm 0.5\text{cm}$$

## C. Spatial Mode Control

### C.1. Theory

A Gaussian wave is a solution to the Helmholtz equation as was stated earlier, but more interesting is the fact that there are separate mathematical functions under the name of Laguerre-Gauss modes which also satisfy the Helmholtz equation. Similarly to a Fourier Series, a single beam can consist of infinitely many Laguerre-Gauss modes in a superposition state [3]. These modes have the general form  $\mathcal{L}_m^l \left( \frac{2p^2}{w^2(z)} \right)$  where  $\mathcal{L}_m^l$  is known as the Laguerre operator, and its general solutions can be solved for with the assistance of the Frobenius method, or through MATLAB17.

### C.2. Methods

In order to find the spatial modes of the laser a hair was placed over an optical component which was mounted on a translation stage on the optical rail. The coupler was positioned to have consistent lasing, and a beam splitter was used to illuminate a 25mm lens which projected the image onto a near wall. The position of the optic was moved between the box and the coupler to isolate individual Laguerre-Gauss modes.



**Fig. 1.**  $TEM_{10}$  Laguerre-Gauss mode projected onto wall



**Fig. 2.**  $TEM_{20}$  Laguerre-Gauss mode

### C.3. Results

When translating the hair along the optical axis there were a handful of different locations that resulted in different TEM modes. There was some trouble with using the micrometer based translation stage to find individual LG modes, so gross movement was used to find the modes. When the optical coupler was positioned 43cm from the box the four modes were found at  $TEM_{10} = 8.25\text{cm}$ ,  $TEM_{20} = 7.05\text{cm}$ ,  $TEM_{30} = 8.20\text{cm}$ , and  $TEM_{40} = 7.35\text{cm}$ . The projections of these modes onto the wall can be seen in Figs. 1-4.

## 3. FIBER OPTIC COUPLING

### A. Spatial Profile of Single Mode Fiber

#### A.1. Theory

Optical fibers can come as either multi-mode or single mode fibers. This means that either many or one Gaussian mode is allowed to propagate in the fiber due to the geometry of the device [2]. A HeNe source will naturally produce a Gaussian beam which should couple into an optical fiber. Two very important aspects of the Gaussian beam are the beam width which is dependent on the propagation distance of the beam, and the

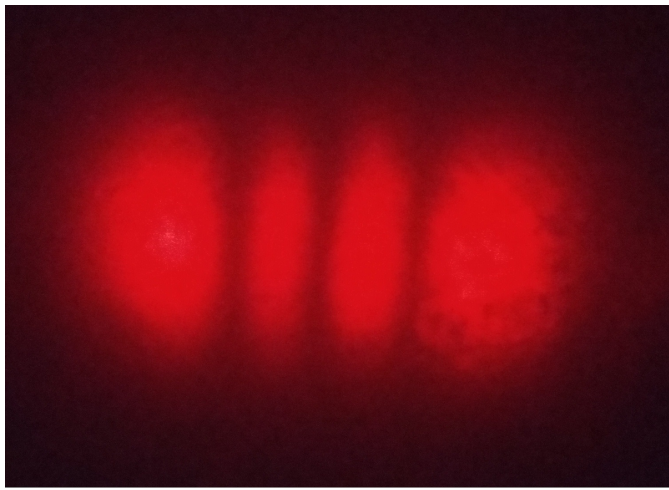


**Fig. 3.**  $TEM_{30}$  Laguerre-Gauss mode

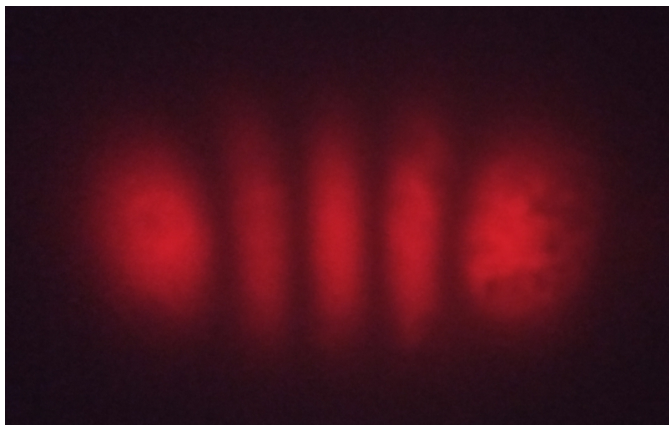


**Fig. 4.**  $TEM_{40}$  Laguerre-Gauss mode

Rayleigh range which describes the distance at which the beam expands by  $\sqrt{2}$  times its initial width [3]. The relationship for the beam waist can be seen in Eq. 2 while that of the Rayleigh range is Eq. 3

$$w(z) = w_0 \sqrt{1 + \left(\frac{z}{z_0}\right)^2} \quad (2)$$

$$z_0 = \frac{\pi w_0^2}{\lambda} \quad (3)$$

If the beam waist of a source is the size of the mode field diameter of an optical fiber the beam will propagate down the fiber with a relatively high efficiency assuming that losses within the fiber are low.

#### A.2. Methods

A single mode fiber was prepared and mounted in front of an  $M^2$  tool with the lowest neutral density filter aperture opened. A HeNe source was used to illuminate a 10x microscope objective which was used to decrease the size of the incident beam before coupling into the optical fiber. The objective was placed at a location which maximized the signal readout by the  $M^2$  tool. The signal was read out by a Thorlabs BC106N-VIS and processed with the accompanying device software which would translate the position of the imaging screen to observe the beam waist as a function of position.

#### A.3. Results

The resultant beam profile which was recorded can be seen in Fig. 5 which expresses the diameter of the beam measured in the x and y direction as a function of the distance from the optical fiber. Assuming that the beam waist is a minimum at the end of the fiber which is located at a stage position of zero, the beam waist solves as:

$$w_0 = 16.21 \mu m$$

Admittedly it would be better to fit the curve to a square root function, but the linear regression which was attempted for this model was too challenging so a quadratic fit was used instead. The mode field diameter of this fiber was about  $4.3 \mu m$  [4] which is about 4 times smaller than the value which was found numerically. This indicates that it probably isn't a good fit, because the beam waist at the fiber should be about the size of the mode field diameter.

Truly this shows a very short stage translation of only 8mm. The stage was about 150mm long, and there should be significantly more data. Unfortunately there seems to have been an issue with data transfer for this portion of the lab as only very small data files were successfully saved onto the Google Drive. In the future it would be beneficial to save all of the data onto an external hard drive just to prevent loss of data.

The Rayleigh range can be found with Eq. 3 as  $z_0 = 1306 \mu m$ .

### B. Gaussian Beam Waist

#### B.1. Methods

Characterization of the laser was carried out with the same device as mentioned in Sec. A. Initially the beam was incident on the device as it was translated along its rail in an effort to capture the beam divergence. After that a 200mm lens was placed 15.5cm from the aperture with the second highest neutral density filter on the device to reduce saturation. The imaging plane was then translated to measure the waist of the beam as a function of position.

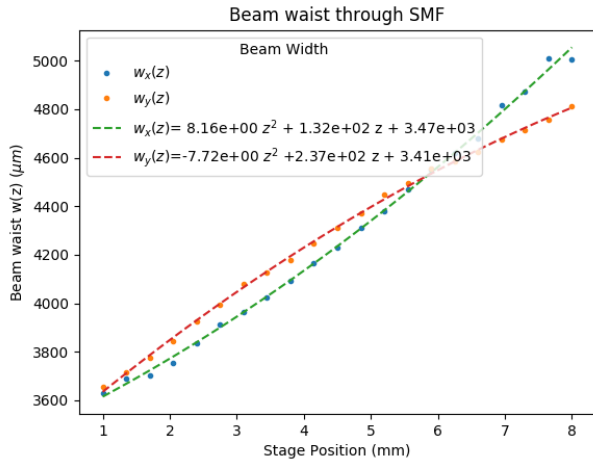


**Fig. 5.** Experimental beam waist measured after propagation through single mode fiber.

A second method for characterizing the beam was carried out by expanding the incoming source which was illuminated onto the same  $200\text{mm}$  lens at a distance  $15.5\text{cm}$  from the imaging plane. The stage was once again translated to capture the divergence of the beam as a function of distance.

## B.2. Results

Unfortunately there was an error while transferring data and it seems that the beam waist which was found by expanding the beam before illuminating the lens wasn't saved properly. Of the remaining data, the Divergence of the HeNe source can be seen in Fig. 7 which shows the beam's waist expanding linearly as it propagates along the optical axis.

A plot of the beam waist after illuminating the lens can be seen in Fig. 6. The beam shrinks from about  $1500\text{ }\mu\text{m}$  to a few hundred microns around  $185\text{mm}$  from the lens. The beam minimum comes down to a width of about  $160\text{ }\mu\text{m}$  which indicates that the value which was calculated in Sec. A for  $w_0$  was potentially off by a decimal place and should be closer to  $160\text{ }\mu\text{m}$ . Also in this figure is the theoretical curve which was found from Eq. 2 and was translated to the minimum position of the experimental data for comparison. The slope of the line seems to be much too high to truly fit the experimental data which indicates that the beam waist was incorrectly calculated in Sec. A which would also mean the Rayleigh range is incorrect. Despite that, the distance from the lens to the fiber which should lead to the highest coupling efficiency can be seen experimentally as the minimum of this experimental curve at about  $185\text{mm}$  from the lens.

## C. Coupling a beam with fiber

### C.1. Methods

The same fiber from Sec. A was placed in front of an optical power meter. A  $200\text{mm}$  lens was placed at a distance  $185\text{mm}$  to couple into the optical fiber. The power of the beam after traversing through the fiber was measured with the power meter. The power meter was then moved to the front of the fiber to find the amount of light which was incident on the front end of the fiber.

In an attempt to optimize the amount of coupling into the fiber, the beam was expanded with a  $-25\text{mm}$  and  $100\text{mm}$  lens

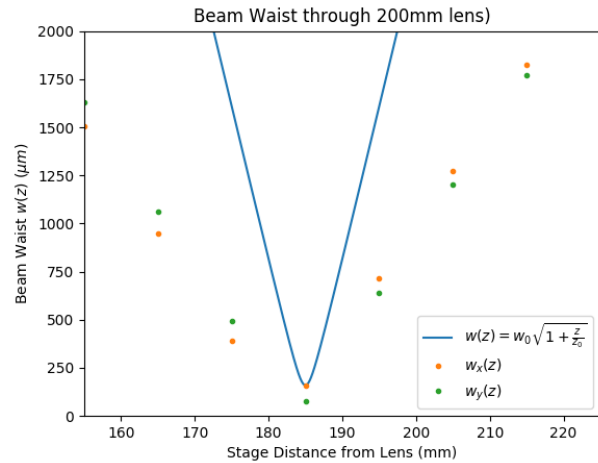


**Fig. 6.** Laser Beam waist measured on  $M^2$  tool after focusing through lens.

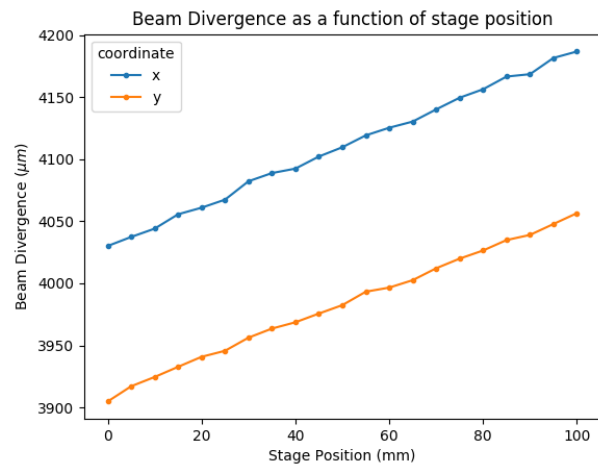


**Fig. 7.** Beam Divergence incident on translation stage.

before illuminating the 200mm lens. The same process was repeated by measuring the amount of power incident on the front of the fiber and compared to the amount of light out of the fiber on the other end.

### C.2. Results

To characterize the coupling efficiency the intensity of the light was captured before entering the fiber and a power of about 1.02W was measured. After the fiber a power of around 27 $\mu$ W was measured. That was an incredibly low efficiency so an investigation was required to determine why there was such a low efficiency because the optical fiber seemed to propagate light much further and in a brighter fashion than previous experiments. The beam was then expanded as described in Sec. C.1, this expanded beam was then used to illuminate the 200mm lens which was placed about 18.5cm from the fiber. The incident power was down to about 185 $\mu$ W and the outgoing power as read by the power meter was around 50 $\mu$ W which indicates a coupling efficiency of 27%. This is a fairly low coupling efficiency still and is much below the 50% desired and the supposed 90% which could hypothetically be achieved.

## 4. CHARACTERIZATION OF AN ACOUSTO-OPTIC MODULATOR

### A. Speed of Sound in the AOM Crystal

#### A.1. Theory

An acousto-optic modulator is a device which contains a small piezoelectric material which oscillates a crystal. The vibrations from the piezo cause phonons to propagate down the crystal and result in regions of compression and expansion of the crystal lattice. These compressions and expansions cause the index of refraction to change as a function of the crystal oscillations. Assuming that the speed of light is much larger than the speed of acoustic vibrations inside of a crystal, the variations in index of refraction behave approximately like a diffraction grating [2]. This allows Eq. 4 to be written.

$$a \sin(\theta) = m\lambda \quad (4)$$

Knowing that the grating spacing  $a$  is related to the driving frequency of vibrations and the speed at which those vibrations can propagate through the crystal, the Bragg equation can be found [3].

$$\sin(\theta_B) = \frac{m\lambda f}{2v_s} \quad (5)$$

Where  $\theta_B$  is the angle at which a diffraction maximum occurs,  $f$  is the driving frequency of acoustic oscillations,  $v_s$  is the speed of sound inside the crystal, and  $\lambda$  is of course the speed of light inside the crystal. For the purposes of this characterization of acousto-optic modulators the speed of light in a vacuum will be used, because the crystal material is assumed to be unknown and thus its index of refraction is also unknown.

#### A.2. Methods

Two separate AOM devices were available to be characterized, one was an IntraAction AOM-402AF3 which will be referred to as AOM1 and the other which will be referred to as AOM2. The first device which was characterized was AOM2 which had a significantly smaller crystal thickness and seemed to be more opaque than AOM1. The experimental setup to determine the speed of sound for the crystal in the AOM can be seen in Fig. 8 where light from a 632.8nm HeNe laser was minified

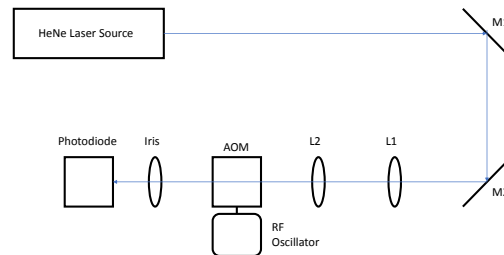


**Fig. 8.** Experimental Setup for determining the speed of sound for the crystal inside the AOM

| AOM2 Diffraction |       |       |   |      |
|------------------|-------|-------|---|------|
| Width (mm)       | 3.5   | 5     | 6 | 4    |
| Position (mm)    | -28.5 | -14.5 | 0 | 15.5 |
| Order            | 2     | 1     | 0 | -1   |

**Fig. 9.** AOM2 Diffraction Table for the beam width and position from the central maximum

with a -25mm lens and 100mm lens to reduce the spot size of the beam to be completely confined within the crystal. The AOM was connected to a driver which produced an 80MHz signal to oscillate the piezoelectric material which was then propagated throughout the crystal. The outgoing light was then filtered through an iris to isolate individual diffraction maxima before illuminating an imaging screen. For AOM1 the imaging screen was moved from 100cm past the to AOM to 50cm in increments of 10cm in an effort to obtain a more accurate relationship between the angle and the speed of sound in the crystal.

#### A.3. Results

The results of diffraction for the first device can be seen in Fig. 9. The iris was removed to allow the entire beam to illuminate the screen, and the width of the four resultant maxima were traced on an index card. The center of each beam was used to note the relative separations from the central maximum which is indicated by Order 0.

The imaging screen was located 1m from the AOM, so the angle of diffraction can be found as  $\sin(\theta_B) = \frac{\Delta y}{1m}$  where the term  $\Delta y$  is the separation between the central maximum and the positions expressed in Fig. 9. With these values the speed of sound can be found from Eq. 5 as,

$$v_s = \frac{m\lambda f 1[m]}{\Delta y} \quad (6)$$

The speed of sound for the crystal in AOM2 can thus be found as,

$$v_s = 3432.3 \pm 123.0[m/s]$$

The same relationship can be used to find the speed of sound for the crystal in AOM1. This results in a speed of sound for that crystal around  $v_s = 8165 \pm 186[m/s]$ .

| AOM2 Deflection Efficiency |                         |                          |                          |
|----------------------------|-------------------------|--------------------------|--------------------------|
| Driver Level               | 0                       | 5                        | 10                       |
| $m = 0$                    | $516 \pm 4 \text{ mV}$  | $555 \pm 3 \text{ mV}$   | $575 \pm 5 \text{ mV}$   |
| $m = 1$                    | $51.0 \pm 2 \text{ mV}$ | $124 \pm 2.0 \text{ mV}$ | $429 \pm 2.0 \text{ mV}$ |
| Efficiency                 | 0.09                    | 0.22                     | 0.75                     |

**Fig. 10.** AOM2 Deflection Efficiency table

## B. AOM Deflection Efficiency

### B.1. Methods

To determine the deflection efficiency of the AOM, the power of the relative maxima need to be measured and compared to the zeroth order beam. The general setup shown in Fig. 8 was used, where the iris and photodetector were moved around to capture light only from the desired intensity maxima. For AOM2 the diffraction efficiency was only captured for a driver frequency of 80MHz, but for AOM1 the driver frequency was changed to determine a relationship between the diffraction efficiency and the frequency of the driver. The amplitude of the diffraction efficiency was also altered to observe how the magnitude of oscillations in the crystal affects the amount of beam diffraction.

### B.2. Results

The same approach was taken to find the deflection efficiency for both devices, but only AOM1 was subject to a range of different driver frequencies to observe those effects. The table shown in Fig. 10 displays the efficiencies which were measured from the photodetector at three different driver amplitudes. There is a clear relationship which shows a higher efficiency is achieved from larger driver amplitudes.

An even better visualization for the relationship between driver amplitude and efficiency is shown in Fig. 11. Five separate frequencies were tested to observe how both the driver frequency and amplitude affect the efficiency. All five curves increase as a function of driver amplitude, but there is a region where the 30MHz driver frequency has a higher efficiency than all other frequencies that were measured. This relationship doesn't hold at maximum amplitude though, as the highest frequency of 45MHz holds the highest efficiency which is then followed by the 30MHz. This curve if carried on to further amplitudes would more than likely asymptote because the vibrations in the crystal would get too large and the material would begin to break down.

## C. Amplitude Modulation of Deflected Beam

### C.1. Theory

Amplitude modulation is a common scheme for signal encoding which is commonly used in radio communication. The general idea is very similar to Fourier series where the amplitude of a single high frequency driving signal is varied to carry the input signal. If however the modulating signal's frequency is too high for the crystal in the AOM to react it can't be resolved.

### C.2. Methods

The device which sends the driving signal to the AOM has a port which allows both amplitude and frequency modulation to be added to the signal which oscillates the piezoelectric in the AOM. A 1Vpp square wave pulse was set to modulate the amplitude of the driving signal at various frequencies. The same general setup shown in Fig. 8 was used with a function generator added to the driver signal of the AOM and an oscilloscope used to read out the signal from the photodetector.

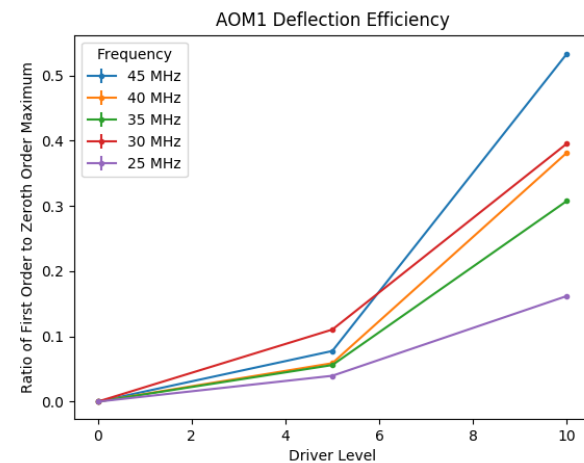


**Fig. 11.** AOM1 Deflection Efficiency for many different driver frequencies

An iris was used to alter the width of the source beam that was incident on the AOM. A better method for this would be to use a variable microscope objective to alter the size of the incident beam, but only a handful of lenses were available at the time and the spot sizes they produced were too large for the crystal. Only AOM1 was used during this characterization because the crystal for AOM2 was significantly smaller and more challenging to use.

To determine the shortest pulse that can be resolved, the zeroth and first order peak intensities on the photodetector were measured with a 10Hz modulation frequency. These intensities were considered the maximum intensity that can be achieved, and the frequency of pulse was changed to find where the intensity dropped to  $-3\text{dB}$  and  $-6\text{dB}$ . This is somewhat of an arbitrary choice, but it would fit to show the frequencies which result in half and quarter intensities. To determine how the driver frequency affects how resolvable the pulses are for a variety of driver frequencies were also tested.

### C.3. Results

The iris was used to change the beam size for two separate cases. The first case had a beam size of 4.5mm and the second had a beam size 3.5mm. When the beam size was decreased below that value the amount of power which was measured on the photodetector was below 25mW and variation of the modulation didn't affect the amount of power read by the detector so any further attempts were abandoned. For the smaller beam an attempt was made to characterize the power in the  $m = 1$  mode but a similar issue occurred where the amount of power in that maximum was just so low that it seemed futile to continue measuring.

A logarithmic plot of the Intensity measured in decibels as a function of the frequency can be viewed in Fig. 12. Large frequency means a shorter pulse in time, and what can be seen is that with a decrease in the spot size a shorter time pulse can be resolved. Interestingly enough the driver frequency didn't show any interesting characteristics so the results were averaged together to represent frequencies and intensities for a particular spot size.

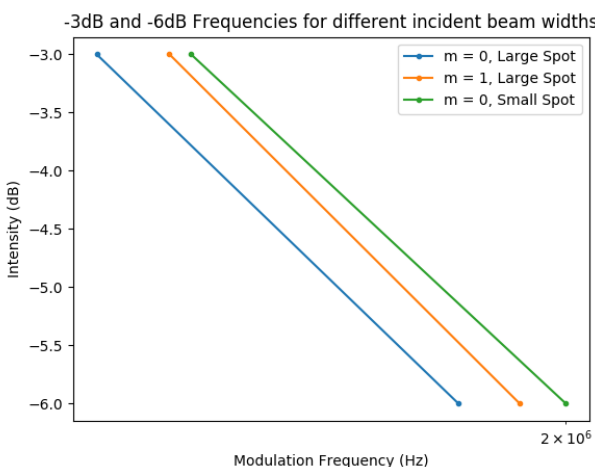


**Fig. 12.** Frequencies corresponding to  $-3\text{dB}$  and  $-6\text{dB}$  from maximum intensity on photodetector

## 5. CONCLUSIONS

### A. Open Cavity He-Ne Laser Recap

Lasing was observed by positioning and properly aligning the optical coupler with the fluorescent beam from an open He-Ne cavity. The range of locations where lasing could occur was tested by moving the coupler up and down the optical axis to observe where lasing began and stopped. It was determined that lasing seemed to occur from the edge of the plastic box holding the cavity, all the way to a distance about 95cm away which indicated mirror curvatures of 42.5cm. Laguerre-Gauss modes were then isolated within the cavity by placing an optical mount with a thin hair at strategic locations to block out all other modes.

### B. Fiber Coupling Recap

An optical fiber was prepared and mounted for light to propagate through it. The beam which made its way through the fiber was incident on a Thorlabs BC106N-VIS  $M^2$  tool which measured the outgoing beam waist and divergence. The smallest beam waist was found to be about  $16\mu\text{m}$  but further investigation indicated that value was off by an order of magnitude and should have been closer to around  $160\mu\text{m}$ . This value was then used to determine the Rayleigh range and the theoretical relationship for the beam waist as a function of distance. The He-Ne beam was passed through a 200nm lens and the beam waist around the focus was measured with the  $M^2$  tool to compare with the theory. Information from the beam profile was used to attempt to couple light into the optical fiber and achieve the highest efficiency possible. There were significant errors in measurement of the efficiency and in the end a low coupling efficiency of about 27% was achieved.

### C. Acousto-Optic Modulator Recap

There were two separate acousto-optic modulators that were available for characterization. They were both used to test for the speed of sound in their respective crystals, where AOM1 had a speed of sound measured to be  $v_s \approx 8000[\text{m/s}]$  and AOM2 measured out around  $v_s = 3500[\text{m/s}]$ . The deflection efficiency for the two devices was also measured with the assistance of a photodiode and a general relationship was found indicating

higher driver amplitudes lead to higher deflection efficiency, but a higher driver frequency doesn't seem to always lead to a higher efficiency. Perhaps there is some interesting resonance effects at particular harmonics that lead to high efficiencies in special frequency regions. Amplitude modulation was also used to find the shortest pulse width that could be resolved from the AOM. A series of different driver frequencies were tested as well as different deflection modes in an attempt to better characterize AOM1. It was found that a smaller incident beam led to shorter resolvable time pulses as was expected, but there was also an indication that higher deflection modes could also result in shorter resolvable pulses and the driver frequency has little to no impact.

In general this document included a discussion of the properties which govern the creation of laser light and Laguerre-Gauss modes which are very important for optical communication. This was followed by the characterization of an optical fiber and the challenges involved with propagating high efficiency signals through single mode fiber. Finishing up, a method for encoding messages into optical fibers was explored with the acousto-optic modulator.

## REFERENCES

1. D. McIntyre, "Lecture notes in physical optics," (2018).
2. S. Mayer, "Lecture notes in physical optics," (2018).
3. B. E. Saleh, M. C. Teich, and B. E. Saleh, *Fundamentals of photonics*, vol. 22 (Wiley New York, 1991).
4. Newport, "Fs-v smf specification sheet," (2018).